ELSEVIER

Ceramics International 28 (2002) 565–573

CERAMICS INTERNATIONAL

www.elsevier.com/locate/ceramint

Interphase effects on the bend strength and toughness of an oxide fibre/oxide matrix composite

Ramanan Venkatesh

School of Materials and Mineral Resources Engineering, Universiti Sains Malaysia, 14300 Nibong Tebal, Seberang Perai Setatan, Pulau Pinang, Malaysia

Received 30 April 2001; received in revised form 12 October 2001; accepted 3 December 2001

Abstract

The effect of alumina–20 wt.% ZrO_2 (PRD-166) fibre and SnO_2 coating properties on the bending strength and toughness of alumina fibre/SnO_2/glass matrix composites have been investigated. The mean strength of as-received alumina–20 wt.% ZrO_2 fibres was 1380 MPa for a gage length of 17 mm and decreased with increase in heat treatment temperatures. It was also observed that as the SnO_2 coating thickness increased, roughness of the coating increased and this decreased the strength of the fibres. This roughness effect had serious implications on the fracture characteristics of PRD-166/SnO_2/glass and Saphikon/SnO_2/glass matrix composites. PRD-166/SnO_2/glass matrix composites exhibited non-planar failure with fiber bridging and fibre debonding as major toughening mechanisms. Saphikon/SnO_2/glass matrix composites failed in a tough manner with extensive fibre pullout. The difference in the failure mode between PRD-166/SnO_2/glass and Saphikon/SnO_2/glass matrix composites was attributed to the clamping stress associated with fiber roughness at the PRD-166/SnO_2 interface as compared to the smoother Saphikon/SnO_2 interface.

Keywords: Interface effects; Bend strength; Toughness; Oxide fibre composite

Introduction

Fibre reinforcement offers a great potential for improving strength and toughness of ceramic materials [1–5]. Parameters that influence the properties of fibres in ceramic matrix composites (CMCs) include: tensile strength, strain to failure, Weibull modulus, aspect ratio and surface roughness. Alumina, mullite and zirconia are the principal polycrystalline oxide fibres developed [6–21]. Oxide fibre/oxide matrix composites are considered for potential use at extremely high temperatures (1400–1600 °C) and in severe environments [22–31]. Failure strength and toughness of CMCs depend on a multitude of mechanisms involving matrix microcracking, matrix prestressing, fibre debonding and fibre pullout. Strength and toughness of CMCs are greatly influenced by the interfacial bonding at the fibre/matrix interface. Interfacial strength is a strong function of the degree of bonding (chemical or mechanical) between fibre and matrix and the thermal mismatch between fibre and matrix. Mechanical bonding is primarily due to irregularities at the fibre/matrix interface. In composites with strong bonding at the interface, cracks originating in the brittle matrix tensile cut through the fibres, resulting in a planar brittle failure of the composite. In a composite with a weak bonding at the interface, when matrix tensile strength is exceeded, multiple cracking of the matrix takes place with the fibres having enough strength to bridge the cracks. Further increase in stress causes fibre debonding due to interfacial stress and Poisson's effect. Continued stressing of the composite beyond fibre debonding causes the failure of the fibre along its length and then depending on residual stress, Poisson's ratio of fibre and matrix and interfacial frictional stress, fibre pullout occurs. Fibre pullout is the main toughening mechanism in CMCs. Hence for a tough composite, the interface bonding should be strong enough to allow load transfer but weak enough to aid crack deflection, fibre debonding and fibre pullout. Interfacial strength can be controlled by modifying the fibre/matrix reactions at the processing and service temperatures either through proper selection of materials or by means of interfacial coatings. For a coating to operate successfully the following conditions should be met.

E-mail address: ram5nan@tm.net.mu (R. Venkatesh).

0272-8842/02/$22.00
PII: S0272-8842(02)00011-1

1. Chemical compatibility with the matrix.
2. Refractoriness.
3. Stability in oxidising, water vapor and corrosive environments.
4. Providing a relatively weak fibre-coating interphase allowing for fibre debonding and pullout.

In oxide fibre/oxide matrix composite systems, reactions at the fibre/matrix interface, e.g. Al_2O_3/SiO_2, mullite/mullite leads to a strong interfacial bonding with the consequence of brittle behaviour of the composite. Various interphase coatings have been applied in oxide fibre/oxide matrix composites including, SnO_2, TiO_2, ZrO_2, HfO_2, monazite, magnetoplumbite, perouskite structures like $BaTiO_3$, etc. [26–33]. In the present work, the effect of fibre and coating properties on the bending strength and toughness of alumina fibre/glass matrix composites have been investigated. SnO_2 was chosen as a coating since it has no reaction with alumina up to 1400 °C in a partial pressure of oxygen $>10^{-7}$ atm. [34,35]. The strength of alumina-zirconia fibres as-received, heat treated and SnO_2 coated were determined. Glass matrix composites fabricated using a slurry impregnation technique and reinforced with two types of fibres, namely PRD-166 (alumina–20 wt.% zirconia) fibres and relatively smooth saphikon fibres were tested to investigate how the properties of the fibres can influence the bending strength and toughness of CMCs.

Experimental procedure

The PRD-166 fiber used in the present work is a polycrystalline α-Al_2O_3 fiber, 20 μm in diameter and containing 15–20 wt.% Y_2O_3 partially stabilized zirconia particles. The properties of PRD-166 fiber are given in Table 1 [36]. The zirconia particles are dispersed throughout the fiber but primarily along the grain boundaries. Saphikon is a single crystal alumina filament. The *c*-axis of the filament is oriented parallel to the fibre surface. The mechanical and physical properties of the saphikon filaments are given in Table 1 [37]. N 51A, a borosilicate glass, obtained from Owens Illinois Inc., was used as a matrix in the present study.

Table 1
Room-temperature properties of PRD-166 fiber and Saphikon filament [36,37]

Fibre	Melting point (°C)	Density (g/cm^3)	Tensile strength (Mpa)	Tensile modulus (GPa)	Thermal expansion ($\times10^{-6}$/°C)
Saphikon	2053	3.9	3150	380	9.12 (// to *c*-axis) 7.95 (to c-axis)
PRD-166	2045	4.2	2070	380	9.0

The alumina (PRD-166) fibres were coated with SnO_2 by a chemical vapor deposition technique. The alumina fibre tows were placed in the central hot zone of the reactor and heated to the deposition temperature of 500 °C. Dry nitrogen was the carrier gas for $SnCl_4$. The flow rate of nitrogen was 1 l/min. A second bubbler contained water heated to 80 °C through which oxygen was passed at a rate of 0.6 l/min. The deposition occurred via the chemical reaction [38],

$$SnCl_4(g) + 2H_2O(g) \rightarrow SnO_2(s) + 4HCl(g) \quad (1)$$

The microstructures of as-received fibres heat treated at 500, 600 and 900 °C for 90 minutes and SnO_2 coated fibres were characterised using SEM and XRD. SEM was used to determine uniformity, morphology and thickness of the coating. The fracture surfaces of the as-received and SnO_2 coated fibres were also characterised by SEM.

Single fibre tensile tests were carried out on as-received, heat treated and SnO_2 coated PRD-166 fibres. A random selection of single fibres was made from the

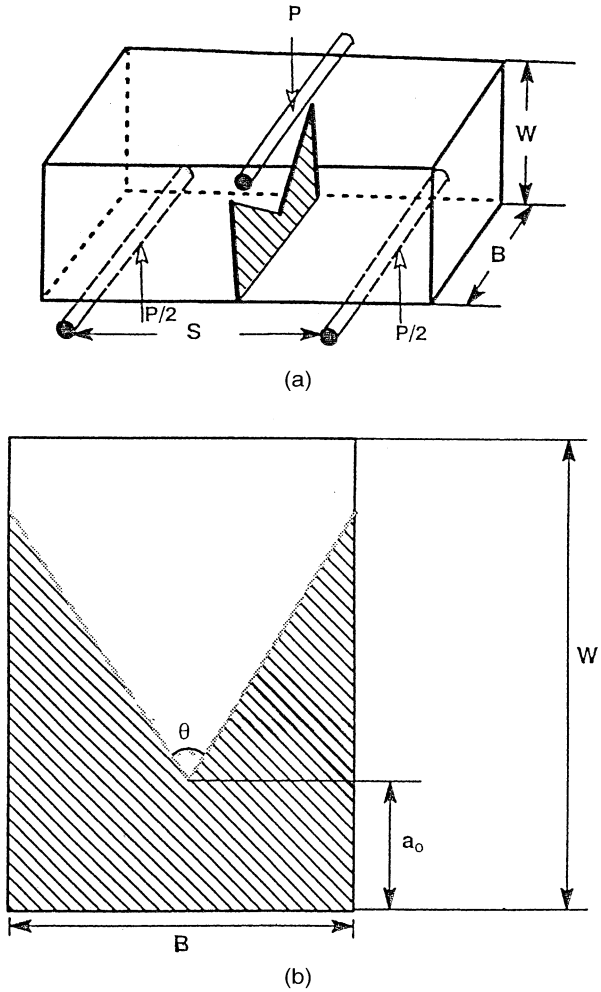

Fig. 1. (a) Chevron notch specimen; (b) geometry of chevron notch.

material to be tested. The fibres were center-line mounted on a paper frame. The fibres were centered over the frame and lightly stretched. A small amount of adhesive was then carefully placed at each end of the fibre. The specimen gage length for all the fibres tested was 17 mm. An Instron tensile testing machine (model 1120) was used with a 5 N load cell. Before fibres were loaded onto the machine, the diameter of the individual fibres was measured with an optical microscope. The frame was then gripped in the jaws of the testing machine and the mounting frame was burned on the sides. The fibres were successively stressed to failure with a crosshead speed of 0.25 mm/min. An average of 80 fibres in each group, i.e. as-received, heat treated at 500, 600 and 900 °C and SnO_2 coated were tested. The mean tensile strength, Weibull modulus, standard deviation and coeffecient of variation were then evaluated by Weibull analysis [39].

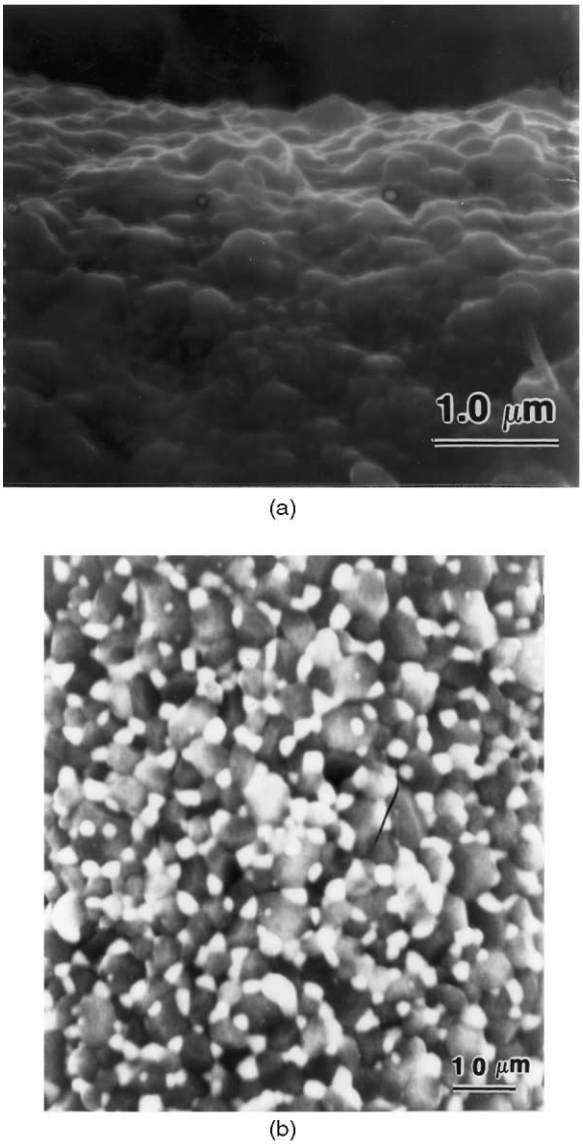

Fig. 2. Microstructure of as-received fibres. (a) Rough longitudinal surface of the fibres; (b) zirconia particles dispersed throughout the fibre.

Alumina fiber reinforced glass matrix composites were fabricated by a slurry impregnation technique [40]. The slurry consisted of glass frit, 2-propanol and an organic binder to impart green strength to the tapes and facilitate their handling. For fabrication of alumina/glass composites, a continuous process was employed to make unidirectional tapes. For fabrication of alumina/SnO_2/glass composites, the coated fibers were dipped in the slurry and laid on mylar tapes to form prepeg tapes. These unidirectional tapes were heated to 500 °C in air to remove the binder and then hot pressed. The hot pressing was performed in a graphite lined die in argon atmosphere at 925 °C and 3 MPa.

Optical microscopy was used to evaluate the volume fraction and fiber distributions in the composites. The fracture surfaces of the composites were characterized using SEM. Three point bending tests on the glass matrix composites were conducted in the longitudinal direction. Bending tests were carried out on specimens having a span length (S) to thickness (W) ratio > 8 and thickness (W) to breadth (B) ratio of 0.75. The three point bending tests were conducted on an Instron machine (model 1102) with a crosshead speed of 0.05

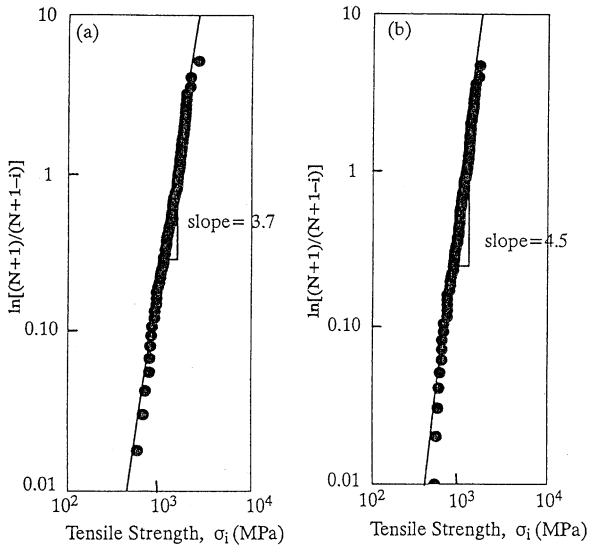

Fig. 3. Weibull plots (a) as-received PRD-166 fibres; (b) SnO_2 coated PRD-166 fibres.

Table 2
Estimated Weibull parameters of as-received and heat treated alumina (PRD- 166) fibres

Fibre	Mean tensile strength (MPa)	Standard deviation (MPa)	Coefficient of variation (%)
As-received	1375	418	30
500 °C	1313	386	29
600 °C	1283	440	34
900 °C	1083	320	29

mm/min. Fracture toughness of all the composites was determined using chevron notch specimens as shown in Fig. (1a). A specimen geometry having a span-to-thickness ratio of 4 and thickness–to-width ratio of 1.5 was used to evaluate the fracture toughness. The three point bending tests were conducted on an Instron machine (model 1102) with a crosshead speed of 0.05 mm/min. The fracture toughness (K_{1c}) was evaluated by the following equation

$$K_{1c} = (P/BW^{1/2})Y_c \quad (2)$$

where P is maximum load, and Y_c is a dimensionless stress intensity factor. From a slice model [41] for the specimen geometry used, Y_c can be evaluated as [42]

$$Y_c = (5.639 + 27.44\alpha_o + 18.93\alpha_o^2 - 43.42\alpha_o^3 + 338.9\alpha_o^4) \quad (3)$$

where $\alpha_o = a_o/W$ and a_o is the initial crack length (distance from line of load application to tip of chevron notch) as shown in Fig. 1(b).

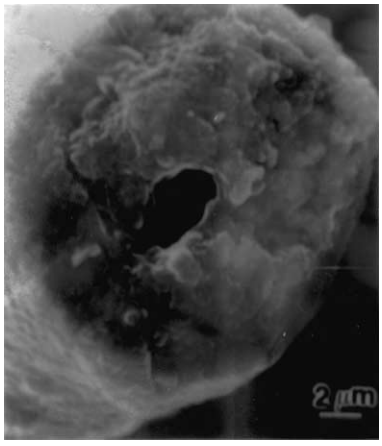

Fig. 4. Fracture surface of an as-received fibre showing processing voids.

Table 3
Estimated Weibull parameters of as-received and SnO_2 coated alumina (PRD-166) fibre

Fibre	Mean tensile strength (MPa)	Standard deviation (MPa)	Coeffcient of variation (%)
As-received	1375	418	30
SnO_2 coated (0.4 μm)	1060	386	25
SnO_2 coated (0.5 μm)	966	440	28
SnO_2 coated (0.8 μm)	851	320	33
SnO_2 coated (2.0 μm)	702	440	32
SnO_2 coated (10 μm)	166	320	34

Table 4
Radial (σ_r), circumferential (σ_θ), and axial stresses (σ_z) at the alumina fibre/SnO_2 interphase. Subscript f denotes the fibre and s the coating

Thickness of SnO_2 (μm)	$\sigma_r f = \sigma_q f = \sigma_r s$ (MPa)	σ (MPa)	$s_z s$ (MPa)	$\sigma_q s$ (MPa)
0.4	22	45	−540	−526
0.5	28	55	−535	−518
0.8	42	88	−524	−497
2.0	53	97	−502	−485

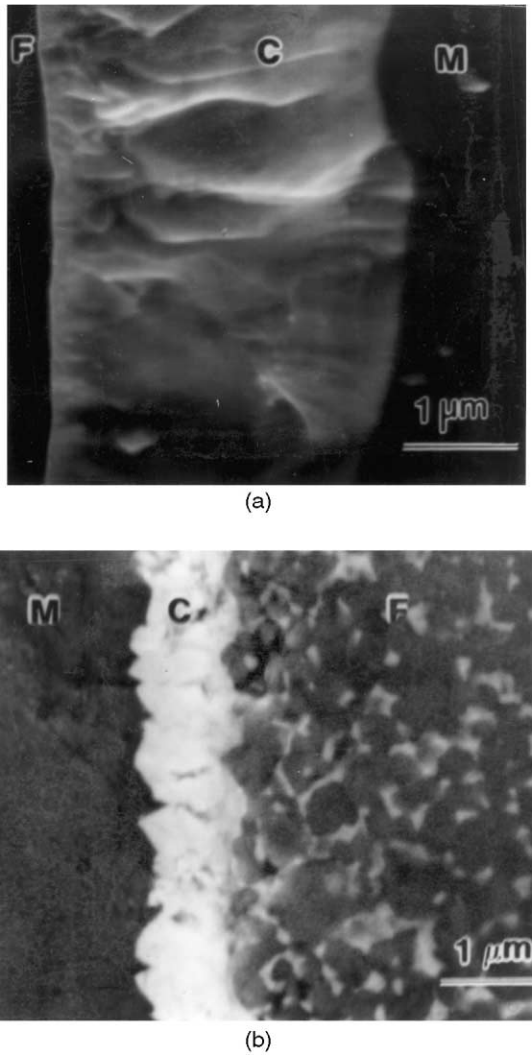

Fig. 5. Interface morphology (a) Saphikon/SnO_2 and; (b) alumina(PRD-166)/SnO_2.

Table 5
Amplitude of roughness, A with coating thickness of the fibres

Thickness of SnO_2 (μm)	Amplitude, μ (mm)
0.0	0.26
0.4	0.45
0.5	0.53
0.8	0.88
2.0	1.8
10.0	4.0

Results and discussion

Fig. 2 (a) and (b) shows the microstructure of alumina PRD-166 fibres. The rough cobblestone surface of the alumina fibres is shown in Fig. 2(a). The zirconia particles are dispersed throughout the fibres but primarily along grain boundaries [Fig. 2(b)]. The dispersion of 20 wt.% zirconia in PRD-166 fibre inhibits grain growth and thereby improves strength and toughness of these fibres [36]. The grain size of alumina, as determined by the lineal intercept method, was about 0.5 μm and that of zirconia particles was 0.33 μm. XRD showed the zirconia particles to be primarily in tetragonal form.

Table 6
Roughness strain A/r compared with thermal mismatch strain of PRD-166/SnO_2 and Saphikon/SnO_2 interphase

	A/r	$\Delta\alpha\Delta T$
PRD-166/SnO_2	0.026	0.0013
Saphikon/SnO_2	0.003	0.001

Weibull plots of as-received and SnO_2 coated fibres are shown in Fig. 3(a) and (b). The straight line plots indicate that the tensile strength data for the as-received and SnO_2 coated follow Weibull distribution. Table 2 shows the tensile strength, Weibull modulus (m), scale

Table 7
Bend strength, WOF and fracture toughness of AG and ASG composites

	V_f (%)	Bend strength (MPa)	Work of fracture (J/m^2)	Fracture toughness (MPa $m^{1/2}$)
	12	110	220	2.0
AG	20	140	–	–
	26	205	420	2.3
	30	215	–	–
	42	230	770	2.6
	24	120	580	2.8
ASG	36	150	900	3.3
	46	190	–	–

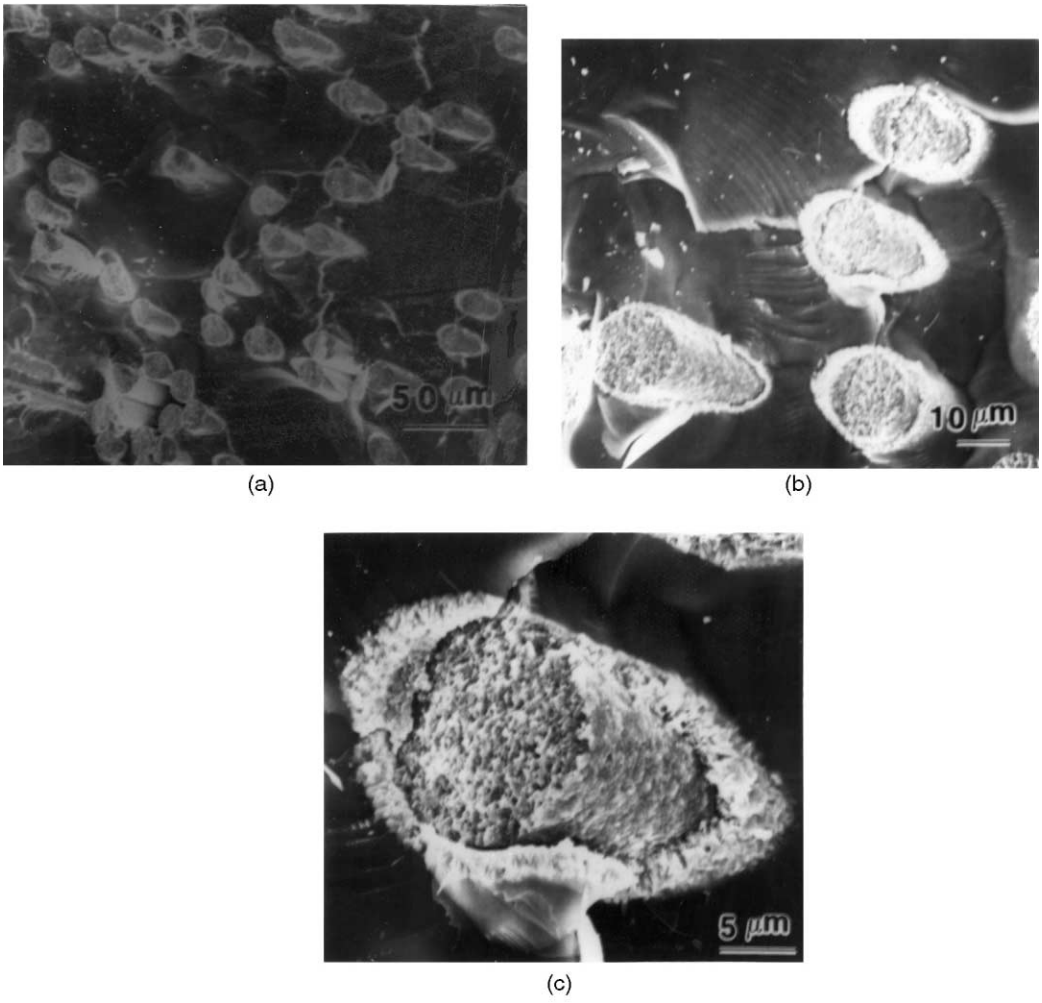

(a) (b) (c)

Fig. 6. (a, b and c) Fracture surface of PRD-166 alumina fibre/SnO_2/glass matrix composites showing partial debonding and fibre pullout. Note the extremely rough PRD-166 fibre.

parameter (α), standard deviation and coefficient of variation of as-received and heat treated alumina fibres. A room temperature strength of 1375 MPa was obtained for a gage length of 17 mm. This value is lower than that reported by Romine [36] who obtained a strength of 2100 MPa for a gage length of 6.9 mm and Yang et al. [43] who obtained a strength of 1180 MPa for a gage length of 50 mm. There are two effects explaining such results: one is the different gage lengths, the other the presence of voids (Fig. 4) in the as-received alumina fibres. As the Weibull strength at a given probability depends on the stressed volume as $V^{-1/\beta}$, for fibres of the same diameter tested on different gage lengths L, L', the strength ratio should be $\sigma/\sigma' = L/L'$; the result of the present research to be compared with the one by Romine is, accordingly, 1375 $(17/6.9)^{1/3.5}$ = 1779 MPa. The value to be compared with Yang et al gives 1375 $(17/50)^{1/3.5} = 1010$ MPa. Both values are lower than measured by the cited authors. The difference in results obtained could be explained by presence of voids. It can also be seen from Table 2 that the strength decreases with increase in heat treatment temperature. Pysher and Tressler [44,45] have reported the presence of minor elements (0.01–0.1%) of Si, and P which could form a SiO_2-P_2O_5 glassy grain boundary phase in PRD-166 fibres at high temperatures. These glassy phase could reduce the strength of the fibres. It has been shown in earlier works that the alumina fibres undergo transgranular failure up to 800 °C beyond which the failure mode is intergranular [44,45].

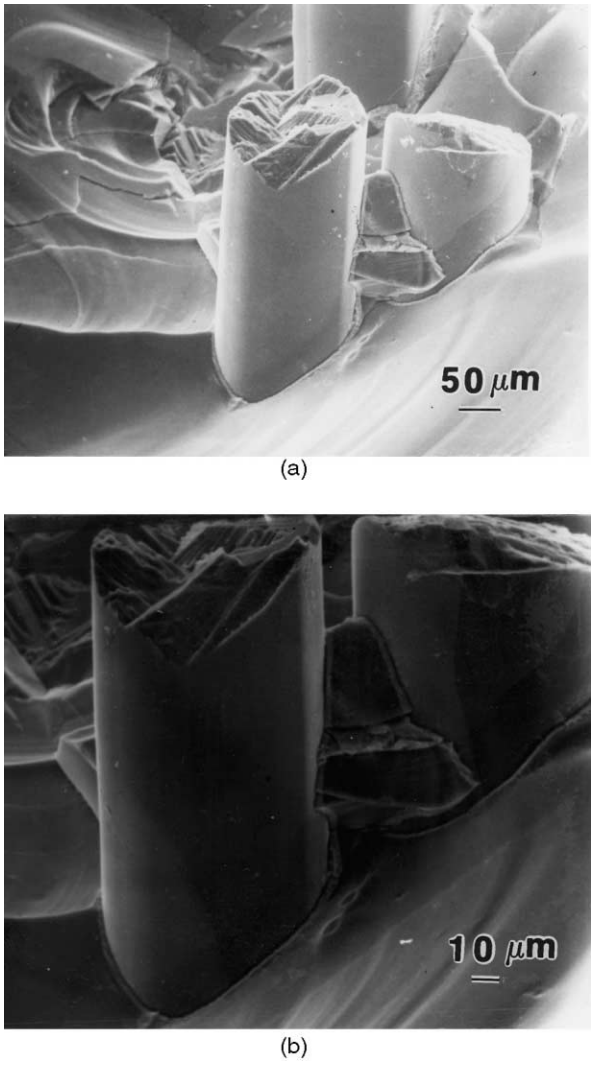

Fig. 7. (a and b) Fracture surface of Saphikon alumina fibre/SnO_2/glass matrix composites. The SnO_2 coating on a relatively smooth saphikon fibre results in a neat a long fibre pull out.

Table 3 shows variation of tensile strength, Weibull modulus and scale paremeters of SnO_2 coated fibres. Again, the tensile strength decreases with increase in coating thickness. Some loss in strength can be attributed to exposures at 500 °C during SnO_2 deposition. Another source of strength reduction could be thermal stresses generated after deposition and subsequent cooling of the alumina/tin dioxide composite fibre. Thermal stresses at the fibre/coating interface were calculated using a two-element cylinderical model [46,47], and the results are shown in Table 4. The radial stress is tensile while the axial and circumferential stresses are tensile in the fibre and compressive in the coating. The axial tensile stress and radial stress increases with coating thickness. This state of stress could reduce the strength of the fibres with increase in coating thickness.

In order to obtain a measure of the effect of roughness on the properties of the fibres, amplitude of roughness of as-received and SnO_2 coated fibres was evaluated. The peak-valley roughness amplitude, A, was evaluated in the present study using SEM micrographs and tracings of roughness profiles. These results are shown in Table 5. It can be seen that the amplitude of roughness, A increases with increase in coating thickness. Under an axial load, this roughness could act as a notch and decrease the strength of the fibres with increase in coating thickness.

The roughness of fibre surface and coating have serious implications in the development of tough ceramic matrix composites. In order to further study the effect of fibre roughness, two different types of fibres namely, alumina fibre (PRD-166) and Saphikon fibre on the fracture characteristics of alumina fibre (PRD-166)/glass (AG), Saphikon fibre/glass (SG), alumina fibre (PRD-166)/SnO_2/glass (ASG) and Saphikon fibre/SnO_2/glass (SSG) composites were investigated. Evaluating compressive roughness strain, A/r (amplitude of roughness/radius of fibre) using tracings of interphase micrographs Fig. 5(a) and (b) it was observed that the A/r value of PRD-166/SnO_2 interface was about nine times that of the Saphikon/SnO_2 interface (Table 6). It was also found that, in PRD-166/SnO_2/glass matrix composites, the compressive radial strain induced due

to fiber roughness was about 20 times larger than the tensile thermal radial strain, $\Delta\alpha\Delta T$. In Saphikon/SnO_2/glass matrix composites, the roughness induced compressive strain was only three times larger than the tensile thermal strain. This indicates the strong mechanical clamping due to fiber roughness at the fiber/SnO_2 interface in ASG composites.

The bending strength of AG and ASG matrix composites as a function of volume fraction of fibers is shown in Table 7. Volume fraction of SG and SSG

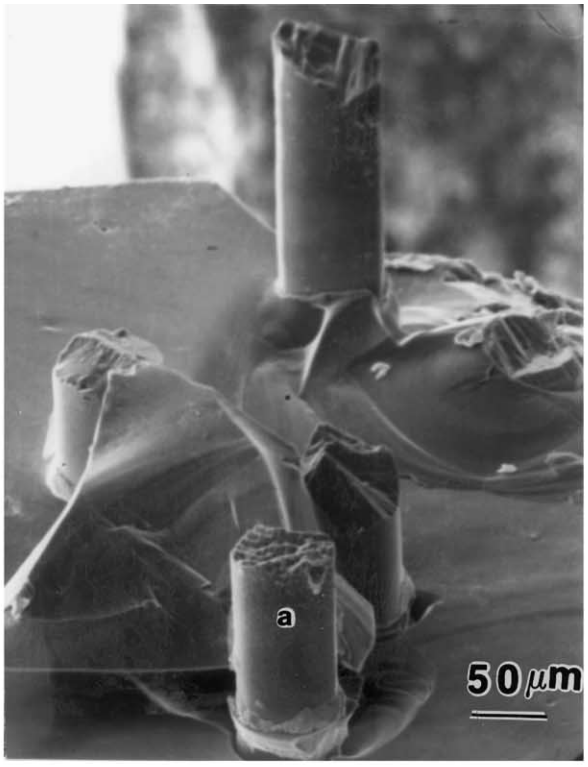

(a)

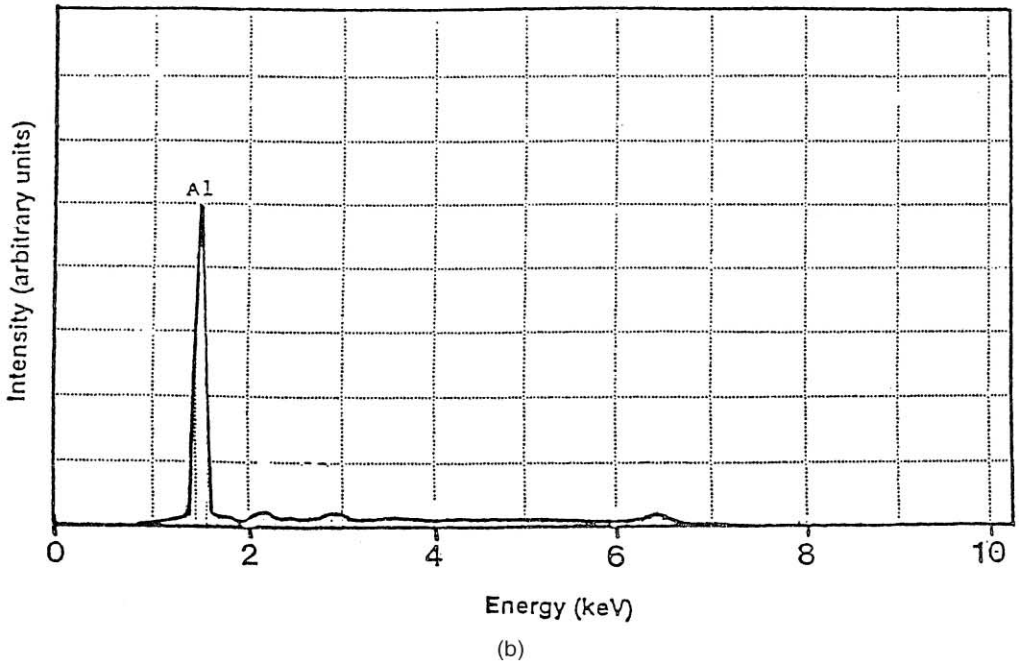

(b)

Fig. 8. (a) Fracture surface of saphikon/SnO_2/glass composites; (b) EDS analysis in region marked (A) showing only Al and no Sn.

composites was only 3%. It should be pointed out that SSG composites were fabricated using a small quantity of fibers only to verify the importance of fiber roughness. The bend strength increased with the volume fraction of the fibers. The strength of AG was slightly greater than ASG, possibly due to the strong chemical bonding at the fiber/matrix interface leading to better load transfer in AG as compared to ASG composites. The work of fracture evaluated from the area under the load-displacement curve for both coated and uncoated composites is shown in Table 7. This parameter increased with volume fraction of fibers in both uncoated and coated fiber composites. The work of fracture of ASG composites was larger than that of AG composites due to contributions from modulus mismatch, crack deflection, fiber bridging and fiber pullout. Fracture toughness as a function of volume fraction of fibers for both AG and ASG composites is shown in Table 7. The toughness of AG composites obtained in this study is in close agreement with that obtained by Michalske and Hellmann [48]. The toughness of AG and ASG composites increased with volume fraction of fibers. The toughness of ASG composites was larger than that of AG composites. The main contributors to the increase in toughness of ASG as compared to AG composites are crack deflection, partial debonding, fiber bridging and partial fiber pullout.

Fracture surfaces of ASG composites are non planar, Fig. 6. Fig. 6 also shows that the predominant mechanism of toughening is fiber bridging and fibre debonding. Partial pullout of fibers can also be seen. A higher magnification micrograph of the fracture surface of ASG composites along the fiber, [Fig. (6c)], shows clearly the partial removal of the coating and the rough fiber surface. Hence the primary toughening mechanisms in ASG composites are crack deflection, fiber bridging, partial fiber debonding and pullout. It has been shown that as the roughness of interphase increases, the compressive clamping stress increases thereby affecting the fracture resistance of ceramic matrix composites [49–58]. This increase in the compressive clamping stress due to fibre roughness causes an increase in the shear stress transfer at the interface beyond matrix cracking from fiber to matrix. This causes a reduction in the debond length, i.e., fibers break rather than debond as the matrix crack grows, resulting in a composite fracture surface in ASG with little or no fiber pullout on the fracture surface Fracture surface of SSG composites, Fig. 7 (a and b), showed neat fiber debonding and fiber pullout at the fiber/SnO_2 interface, as confirmed also by EDS on the pulled out saphikon fiber in Fig. 8. In the region marked as a, the EDS analysis showed only Al and no Sn since SnO_2 and Al_2O_3 have no mutual solubility. Hence fibre debonding and fibre pullout with lengths over 100 μm take place in saphikon fibre/SnO_2/glass matrix composites. Thus interfacial roughness plays a major role in the fracture resistance of ceramic matrix composites. Interfacial roughness in CMCs can be controlled through the use of smooth fibres or reducing the coating thickness.

Conclusion

1. The strength of alumina–ZrO_2 fibres (PRD-166) decreased with increase in heat treatment temperature of fibres. This could be because of the presence of a glassy second and/or due to processing defects in the fibres.
2. The strength of the fibres decreased with increase in SnO_2 coating thickness. It was observed that as the coating thickness increased, roughness of the coating increased. This acted as a notch in order to decrease the strength of the Al_2O_3/SnO_2 composite fibres.
3. In CMCs, as roughness increased, fibre debonding decreased and toughness of composite decreased. PRD-166/SnO_2/glass matrix composites exhibited non-planar failure with fiber bridging and debonding as major toughening mechanisms. Saphikon/SnO_2/glass matrix composites failed in a tough manner with extensive fiber pullout.
4. The difference in the failure mode between PRD-166/SnO_2/glass and Saphikon/SnO_2/glass matrix composites could be attributed to roughness of the fibres.
5. It is important to control the roughness at the fibre/coating and coating/matrix interfaces in order to develop tough ceramic matrix composites. Methods of decreasing roughness at the interfaces consist in the incorporation of smooth fibres and in decreasing coating thickness.

References

[1] I.W. Donald, P.W. McMillan, J. Mater. Sci. 11 (1976) 146.
[2] R.W. Rice, Ceramic matrix composite toughening mechanisms: an update, in Ceramic Science and Engineering Series, Vol. 6, American Ceramic Society, Columbus, OH, p.589.
[3] A.G. Evans, Perspective on the development of high-toughness ceramics, J. Am. Ceram. Soc. 73 (1990) 187.
[4] W.B. Hillig, Strength and toughness of ceramic matrix composites, Ann. Rev. Mater. Sci. 17 (1987) 341.
[5] D.B. Marshall, J.E. Ritter, Reliability of advanced structural ceramics and ceramic matrix composites–a review, Ceram. Bull. 66 (1987) 309.
[6] H.G. Sowman, D.D. Johnson, in: K.S. Mazdiyani (Ed.), Fibre Reinforced Ceramic Composites: Materials Processing and Technology, Noyes Publications, USA, 1990, pp. 122–138.
[7] G. Das, Ceram. Eng. Sci. Proc. 16 (5) (1995) 977–986.
[8] G. Das, Ceram. Eng. Sci. Proc. 18 (6) (1997) 25–33.

[9] D.M. Wilson, D.C. Luenberg, S.L. Lieder, Ceram. Eng. Sci. Proc. 14 (1993) 7–8.
[10] D.M. Wilson, D.C. Luenberg, S.L. Lieder, Ceram. Eng. Sci. Proc., 16(5) (1995) 1005–1014.
[11] J.A. DiCarlo, S. Dutta, in: R. Lehmanm, S. El-Rahaiby, J. Wachatman Jr. (Eds.), Handbook on Continuous Fibre Reinforced Ceramic Matrix Composites, CIAC, Purdue University, IN, 1995, 137–183.
[12] R. Venkatesh, Mater. Sci. Eng. A268 (1999) 47–54.
[13] M.H. Stacey, Br. Ceram. Trans. 87 (1988) 168–172.
[14] E. Rasterrer, W.K. Symes, Interceram (1983) 215–220.
[15] J.D. Birchall, Br. Ceram. Soc. 82 (1983) 143–145.
[16] T. Yogo, H. Iwahara, J. Mater Sci, 26 (1991) 5292–5296.
[17] W. Gaubitt, W. Watzke, Scholz, D. Sporn, J. Sol–Gel Sci. Technol. 8 (1997) 29–33.
[18] J. Dinwoodie, Canadian Ceram. Quarterly 2 (1996) 23–29.
[19] A.R. Bunsell, H. Berger, Compos Sci. Technol. 51 (1994) 127–133.
[20] R. Venkatesh, S.R. Ramanan, J. Eur. Ceram. Soc. 20 (2000) 2543–2549.
[21] R. Venkatesh, L.C. Teck, Z.A. Ahmad, A. Fauzi, J. Mater. Tech. 16(2) (2001) 103.
[22] C.G. Levi, J.Y. Yang, B.J. Dalgeish, F.W. Zok, A.E. Evans, J. Am. Ceram. Soc. 81 (8) (1998) 2077–2086.
[23] R. Lundberg, L. Eckerbar, in: R. Naslain (Ed.), High Tech. CMCs II, Woodhead Publ., NY, 1994, pp. 95–103.
[24] R.N. Singh, M.K. Brun, Ceram. Eng. Sci. Proc. 8 (1987) 636–643.
[25] O. Yeheskel, M.L. Balmer, D.C. Cranmer, Ceram. Eng. Sci. Proc. 9 (1988) 687–694.
[26] R. Lundberg, L. Pejryd, E. Butler, M. Kelund, M. Nygreen, in: R. Naslain, L. Doumeingh (Eds.), Proc. Int. Conf. on HTCMC-I, Woodhead Publ., UK, 1993, pp. 167–174.
[27] P.E.D. Morgan, D.B. Marshall, J. Am. Ceram. Soc. 78 (1995) 1553–1563.
[28] M.K. Cinnibulk, Ceram. Eng. Sci. Proc. 16(5) (1995) 721–728.
[29] M.K. Cinnibulk, Ceram. Eng. Sci. Proc. 15(5) (1994) 721–728.
[30] K.K. Chawla, Z.R. Xu, R. Venkatesh, J.S. Ha, 9th Int. Conf. on Composites, Spain, 1993, pp. 789–795.
[31] R. Venkatesh, P.K. Chakrabarthy, B. Siladitya, M. Chatterjee, D. Ganguli, Ceram. Int. 25 (1999) 539–543.
[32] J.B. Davis, J.B. Lofrander, A.G. Evans, E. Bischoff, M.C. Emiliano, J. Am. Ceram. Soc. 76(5) (1993) 249–257.
[33] R. Venkatesh, K.K. Chawla, J. Mater. Sci. Lett. 11 (1992) 650–653.
[34] P.E.D. Morgan, D.B. Marshall, J. Am. Ceram. Soc. 78 (6) (1995) 1553–1556.
[35] K.K. Chawla, A. Choudhary, R. Venkatesh, J.R. Hellmann, Mater. Char. 31 (3) (1993) 167–172.
[36] J.C. Romine, Ceram. Eng. Sci. Proc. 8 (1987) 1755–1760.
[37] Saphikon data sheet, Saphikon, NH.
[38] G.N. Advani, A.G. Jordan, C.H.P. Lupis, R.L. Longini, Thin Solid Films 62 (1979) 361–369.
[39] W. Weibull, Appl. Mech. Rev. 5 (1952) 449–454.
[40] K. Prewo, J.J. Brennan, G.K. Layden, Am. Ceram. Soc. Bull. 65 (1980) 305–312.
[41] J.I. Bluhm, Eng. Fract. Mech. (1984) 221–225.
[42] Wu-Shang Xian, Eng. Frac. Mech. 19 (1984) 271–276.
[43] X. Yang, X. Hu, R.J. Day, R.J. Young, J. Mater. Sci. 27 (1992) 1409–1416.
[44] J. Pysher, K.C. Goretta, R.S. Hodder, R.E. Tressler, J. Am. Ceram. Soc. 72 (2) (1989) 284–288.
[45] D.J. Pysher, R.E. Tressler, J. Mater. Sci. 27 (1992) 423–428. 65.
[46] H. Poritsky, Phy. 5 (1934) 406–410.
[47] A.W. Hull, E.E. Burger, Phy. 5 (1934) 384–389.
[48] T.A. Michalske, J.R. Hellmann, J. Am. Ceram. Soc. 71 (1998) 725–732.
[49] T.A. Parthasarathy, R.J. Kerans, J. Am. Ceram. Soc. 80(5) (1992) 2043–2055.
[50] C.H. Hseuh, J. Mater. Sci. Lett. 16 (5) (1997) 350–358.
[51] R.J. Kerans, T.A. Parthasarathy, J. Am. Ceram. Soc. 74 (1991) 1585–1600.
[52] T.J. Mackin, J. Yang, P.D. Warren, J. Am. Ceram. Soc. 75(12) (1992) 3358–3365.
[53] T.A. Parthasarathy, R.J. Kerans, J. Am. Ceram. Soc. 80 (8) (1992) 2043–2501.
[54] H.P. Wang, C.L. Nelson, C.L. Lim, W.W. Gerberch, Interfacial stability and mechanicxal properties of alumina fibre reinforced Ti matrix composites, J. Mater. Res. 9 (2) (1994) 498.
[55] P.D. Jero, T.A. Parthasarathy, Interface properties their measurement with fibre pushout tests, in R. Naslain (Ed.), High temperature Ceramic Matrix Composites, Goodhead Publishers, Cambridge, 1993, p. 401.
[56] B.F. Sorensen, Effect of fibre roughness on the overall stress–transverse strain response of ceramic composites, Scripta Metall. Et Mater. 28 (1993) 435.
[57] W.C. Carter, E.P. Butler, E.R. Fuller Jr., Scripta Metall. Mater. 25 (1991) 579–585.
[58] T.J. Mackin, P.D. Warren, A.G. Evans, Acta Metall. 40 (1992) 1251–1259.